Materials Research. 2018; 21(2): e20170210
DOI: http://dx.doi.org/10.1590/1980-5373-MR-2017-0210

Corrosion Resistance Evaluation of HVOF Produced Hydroxyapatite and TiO_2-hydroxyapatite Coatings in Hanks' Solution

Hortensia Correas Melero[a], Rafael Toshio Sakai[b], Claudia Abellan Vignatti[a], Assis Vicente Benedetti[c], Javier Fernández[a], Josep Maria Guilemany[a], Patricia Hatsue Suegama[b]*

[a]Centre de Projecció Tèrmica - CPT, Universitat de Barcelona, Martí i Franquès 1, 08028, Barcelona, Spain
[b]Faculdade de Ciências Exatas e Tecnologia, Universidade Federal da Grande Dourados - UFGD, Rodovia Dourados - Ithaum km 12, 79825-070, Dourados, MS, Brazil
[c]Departamento de Físico-Química, Instituto de Química, Universidade Estadual Paulista - UNESP, Rua Prof. Francisco Degni, 55, 14800-060, P.O. Box 355, Araraquara, SP, Brazil

Received: February 21, 2017; Revised: October 18, 2017; Accepted: December 05, 2017

The electrochemical behavior of HVOF produced hydroxyapatite (HA) and 80HA-20TiO_2 coatings were investigated using electrochemical techniques in natural aerated Hanks' solution in the presence and absence of bovine serum albumin (BSA) for 30 days. All samples presented open circuit potential oscillations, which were associated to the porous nature of the coating that allows the electrolyte reaches the substrate causing activation - passivation at the bottom of the pores. The polarization studies indicated that the 80HA-20TiO_2 coating was the only one that showed a narrow potential passive region from around -0.4 V to 0 V in the presence and absence of BSA, indicating the beneficial influence of the addition of TiO_2 to the HA coating stability. Our results indicated that BSA in Hanks' solution diminishes the stability of the metallic oxide layer present on the Ti-based alloy accelerating the degrading of hydroxyapatites coatings / substrate interface due to its chelating ability.

Keywords: *HVOF, hydroxyapatite coating, TiO_2-hydroxyapatite coating, TiAlV alloy, BSA.*

1. Introduction

Titanium can be alloyed with other corrosion resistant materials in order to improve the corrosion stability of titanium [1]. Firstly, developed for aerospace industry, the Ti-6Al-4V has been extensively used as medical orthodontic implants. Once it is bioinert, its osseointegration process is too slow and can be improved using a biocompatible coating. Hydroxyapatite (HA), a bioactive and osseoconductive material, which promotes direct attachment to bone, has been widely used for surface improvement of the metallic implants due to its great biocompatibility with body fluid, but it lacks of good mechanical proprieties [2,3]. Its arrangement with other compounds such as carbon nanotubes, ceramic or other components has been deemed to overcome this weakness [4-6].

Thermal spraying processes are the fastest method to deposit HA coatings with good adhesion to the substrate. HA coatings prepared by plasma spraying may have problems of long-term stability due to their higher degree of porosity, poor bond strength, presence of a small amount of amorphous phase with non-stoichiometric composition, and non-uniformity [7]. High Velocity Oxygen Fuel (HVOF) sprayed coatings are attractive for corrosion resistance, because they are dense and exhibit low oxidation of raw materials compared to coatings obtained by other thermal spray processes (plasma or wire arc spray) [8]. In addition to the good adhesion, these coatings presented positive results for bone growing either *in vitro* or *in vivo* testing [9-12].

Almost one hundred of works has been published dealing with the electrochemical, corrosion and/or mechanical properties of HA-based coatings applied on different substrates and produced by means of different techniques. The electrochemical characterization was largely done by open circuit potential (E_{OCP}) measurements and potentiodynamic polarization: lineal, Tafel and cyclic polarization [1,7,13-25]. Tafel and cyclic polarization are good techniques for many studies but have the drawbacks to be destructive techniques due to the high potential polarization imposed which can damage the sample.

However, a small number of studies used electrochemical impedance spectroscopy (EIS), and a few of them measured the impedance of the HA-Ti and its alloys system for times longer than 48 hours immersion [13,18,26], which means that the characterization of the electrochemical behavior of many HA coatings should be investigated in more detail concerning their electrochemical. The EIS has the advantage of to be a non-destructive and transient technique, is able to separate the resistance of electrolyte from the processes occurring at the electrode/electrolyte interface, explores a great frequency range allowing to detect events occurring in a large time constants interval [27-29]. Curiously, works recently

*e-mail: pattyhs@gmail.com

published[30-33] using plasma spray, microplasma, and vacuum cold spray to deposit hydroxyapatite for biological purposes have studied different properties, but no electrochemical investigation was performed.

The addition of BSA to the Hanks' solution or in any simulating body fluids changes the electrochemical behavior of metallic implants [15,34,35] mainly due to two effects attributed to BSA: adsorption and chelating. The BSA molecules have the ability to adsorb on metal surface [35]. The adsorption of BSA on metallic surfaces makes the rate of the oxygen reduction reaction decreases, and consequently, moves the open circuit potential to lower values, since the access of oxygen to the active sites of the electrode may be hindered. Therefore, the rate of the cathodic reaction decreases and consequently the open circuit potential also decreases [15], which makes smaller the corrosion rate. The local cell theory [36] has been evoked to explain the passivation o the bottom of the pores present in many coatings, but in the presence of BSA the local cell theory is still valid, however the chelation of calcium from calcium phosphate deposits may avoid the surface passivation [15], resulting in enlargement of pores and increase of corrosion.

Thus, the aim of this work is to evaluate the corrosion behavior of the HA and compare with an 80-20wt% HA/TiO_2 coating, as well investigate the influence of BSA on the stability of the coating surface in Hanks' solution providing physical models to a fully understand of the corrosion progress for 30 days.

2. Experimental Procedure

A Ti-6Al-4V alloy was used as substrate and previous the spraying process, it was degreased and grit blasted with corundum to get a rough surface with a mean roughness around 5 µm, and sufficient anchorage points between the sprayed coating and the substrate.

A spherical commercial hydroxyapatite powder, with particle size of (31 ± 2) µm and irregular commercial rutile powder, with particle size of (31 ± 2) µm were sprayed using a HVOF technique by means of a Sulzer-Metco DJH 2600 HVOF system. Propylene was used as the fuel gas and compressed air as carrier gas. Two coatings were obtained: pure HA coating and 80-20wt% HA-TiO_2, respectively (80-20). Table 1 shows the spraying parameters used to obtain the both coatings and also the thickness of the coatings estimated from the cross section SEM images. The estimated porosity, obtained from SEM image analysis, was 8 - 12% for both coatings. Detectable cracks were also found in the SEM images. A grit blasted substrate and the as-sprayed coatings were employed as working electrode without further surface preparation.

Table 1. Spraying parameters used to build up the coatings and coatings thickness.

	HA	80-20
Oxygen (L min^{-1})	278	265
Propylene (L min^{-1})	81	81
Compressed air (L min^{-1})	203	264
Oxygen/propylene (L min^{-1})	3.96	3.96
Number of layers	7	5
Spraying distance (mm)	240	200
Feed rate (g min^{-1})	25	25
Tranverse speed (mm min^{-1})	500	500
Coatings thickness (µm)	117±9	112±15

The corrosion resistance of coated and uncoated substrates was evaluated by means of electrochemical measurements carried out in an 80 mL three-electrode conventional electrochemical cell with exposing area of 0.74 cm^2 to the solution. A commercial Hanks' solution (Sigma Chemical Co., pH≈7.4) with and without 4.2 g L^{-1} of BSA (Sigma Chemical Co.) was used as electrolyte. An $Ag/AgCl/KCl_{3M}$ electrode, connected to the working solution through a Luggin capillary, was used as reference, and a Pt network as auxiliary electrode. Open circuit potential (E_{OCP} *versus* time), linear polarization (LP) and cyclic polarization (CP) were performed using a PAR EG&G model 263, and electrochemical impedance spectroscopy (EIS) measurements were carried out using a potenciostat-galvanostat Irvium, model VERTEX equipped with an impedance modulus.

For E_{OCP} *versus* time experiments, the electrode has been immersed in Hanks' solution with or without BSA and the potential was measured for 24 h in order to reach a steady-state value. Afterwards, three LP curves have been recorded at 0.166 mV/s with a potential interval of ±20 mV/E_{OCP} in order to obtain the polarization resistance (R_p) values. After the LP measurements, the cyclic polarization curves were recorded starting the polarization scan at -0.200 V/E_{corr}, and once +2.0 V/E_{corr} was reached, the direction of scanning has been reversed, and it has been maintained in the cathodic direction until 1 V below the E_{corr}. The E-log (i / A cm^{-2}) plots were represented until +1.5 V in the reverse scan for practical reasons. The employed scan rate for the entire test has been 5 mV/s. Previous studies of coated and uncoated TiAlV alloys used scan rates from ~0.1 to 10 mV/s to evaluate the corrosion behavior of this system [12,13,18,19], and in many studies high anodic potentials were employed. For all systems, the results are given based on the geometric area, but it is important to mention that the real area can be much higher since as-sprayed samples were used without surface polishing, and therefore, with a relatively high surface roughness.

The electrode was maintained in contact with the solution for 24 h and then the EIS experiment was initiated. E_{OCP} was measured each 24 h for 30 days immediately before and after to conduct each EIS experiment. Both E_{OCP} values were similar (3 mV difference). The EIS diagrams were acquired for immersion times up to 30 days and performed by applying

a 10 mV (rms) sinusoidal perturbation signal to the E_{OCP}, from 1 x 10^5 to 1 x 10^{-3} Hz recording 10 points per frequency decade. During all process, all working electrodes were kept immersed into the study solution. All electrochemical tests were performed at 37 ºC. All experimental data were tested for consistency with the Kramers-Kronig transform, and only those points passing the test are presented and discussed in the paper.

Scanning electron microscope (SEM) images were acquired before and after the potentiodynamic polarizations using a Jeol JSM-840 equipment.

3. Results and Discussion

3.1 Open circuit potential and polarization studies

Although the majority of studies only employed short periods of open-circuit before initiating the electrochemical measurements, it has been considered more appropriate to wait for 24 hours, since the studied materials did not show a stabilization of the electrode/solution interface for shorter times of immersion. Similar behavior was recently observed for HA-based coatings deposited by plasma sprayed technique, and the electrochemical measurements were performed only after 24 hours of immersion [22].

Open circuit potential *versus* time curves representative of freshly as-grit blasted bare and as-sprayed Ti-6Al-4V alloy (HA and 80-20)-coated samples in contact with naturally aerated and unstirred Hanks' solution with and without BSA in solution for 24 hours and at 37 ºC are depicted in Figure 1.

All samples presented some small potential oscillations, which are normally associated to activation - repassivation process (pit formation may also cause oscillation, but here no pits are formed) or the presence of porous film. The presence of pores, in the coating system, is probably the main reason for potential oscillations and also for their lower open circuit potential compared to the uncoated samples. Corrosion

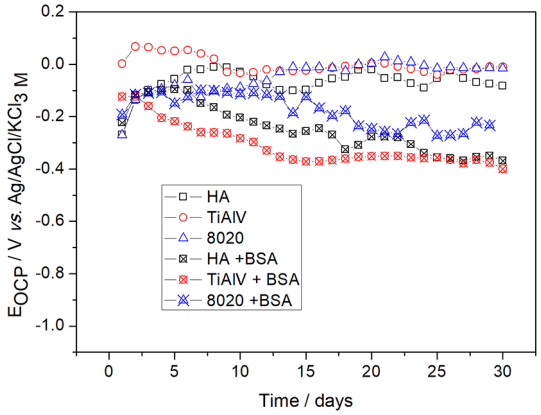

Figure 1. Open circuit potential *vs.* time curves for studied samples in non-deaerated and unstirred Hanks' solution at 37 ºC, with and without BSA for 30 days of immersion.

with simultaneous fretting studies [37] also demonstrated that the potential oscillations can be generated by applying and removal load under rubbing due to the removal of the passive oxide layer, generating an activation-repassivation process. Furthermore, according to literature [25], thick HA coatings showed large potential variations, that in fact can also be observed in our results, owing to the existence of a diffusion path inside the coating, it means porosity [13].

The bare electrode presented the highest E_{OCP} value since this surface spontaneously developed an oxide film. The uncoated sample, in the absence of BSA showed a rapid increase of the potential at initial times of immersion and tended to reach an almost steady-state value at around -0.17 V. Milosev and co-workers mentioned that the oxide layer on top of TiAlV is mainly to TiO_2 with small amount of TiO and Ti_2O_3 near the metal/oxide interface, and that Al as Al_2O_3 and V oxides with different oxidation states can also be present in TiO_2 matrix [38]. Moreover, Cheng and Roscoe, and Pouilleau and co-workers concluded that freshly Ti surfaces exposed to air spontaneously form thin metallic oxide film also composed of TiO, Ti_2O_3 and TiO_2, the last in contact with the solution [15,34]. A similar behavior must occur when freshly TiAlV alloy is placed in contact with air. After the electrode immersion into the solution, the metallic oxide film grows increasing the corrosion resistance, which decreases the rate of anodic current reactions and move the open circuit potential to more positive value. As consequence, the cathodic reaction rate decreases and the resulting open circuit potential (resulted from both anodic and cathodic reactions) may achieve an almost stable potential value.

In the presence of BSA, the potential also reached ~-0.17 V very fast, remained at this value up to around 5.5 h, then decreased and tended to stabilize around -0.22 V. The result suggests that some modification on the electrode surface occurred, probably by modifying the cathodic reaction rate as already observed [15]. The rate of the oxygen reduction decreased, which moved the open circuit potential to lower values, if the access of oxygen to the active sites of the electrode was hindered. It can occur due to the ability of BSA in being adsorbed on metal surfaces [35], which could difficult the access of dissolved oxygen to the electrode surface. On the other hand, the chelating ability of BSA towards metals ions could increase the anodic reaction rate which also would increase the metal dissolution. The effects of BSA on both anodic and cathodic processes lead to a more negative open circuit potential in the presence of BSA [15].

The deposition of HA on the Ti-6Al-4V shifted the E_{OCP} to more active values in the following order: bare Ti-6Al-4V > 80-20 > HA.

For HA-coated samples the potential increased up to around 6 h immersion, then decreased slowly to reach an almost stable potential value at around -0.35 V in the presence and absence of BSA after 24 hours immersion. It would be expected that HA, an inert material, when applied

on the substrate surface will move the E_{OCP} to nobler values [7,14,16-18,25,39,40]. This behavior can be explained because of the dissolution of the amorphous phase that occurred in these coatings during the first 24 hours and produced an increase of the porosity as time goes by [41]. The electrolyte may then achieve the substrate across the coating, forming a local cell, according to Lavos-Valereto and co-workers [36], that induced the latter corrosion. The formation of local cells has been evoked to explain the higher activity of surfaces covered with porous film or coatings whereas proton is formed by a corrosion reaction of the substrate (Ti for instance) with water on the bottom of the pore; the pH decreases locally due to the fact that H^+ is almost closed at the interface due to the difficulty to go away; and in a second step the proton dissolves the HA near substrate/HA interface, probably beginning by the dissolution of the amorphous phase [42].

The E_{OCP} of the 80-20 sample stabilized at around -0.22 and -0.32 V in the absence and presence of BSA, respectively. In our case the sample 80-20 has around 14% and the HA around 20% of amorphous phase, which can produce lower quantity of protons in the local cells resulting in a higher potential compared with HA sample. On the other hand, we must also consider the increase of the E_{OCP} by the contribution of the 20wt%TiO_2 present onto the surface of the 80-20 sample.

Both 80-20 and HA samples immersed in BSA-containing solution presented lower E_{OCP} values than their correlates immersed in Hanks' solution. The hypothesis of the formation of local cells, mentioned above, is still valid in the presence of BSA. Adsorption and chelating effects of BSA must be now considered. As BSA adsorbs on the coating surface, it is probable that some active sites of the oxide surface are less accessible to the oxygen and/or the amount of oxygen inside the pores of the coatings decreases. It polarizes the cathodic reaction, resulting in a decrease of the open circuit potential. The negative charge on the BSA could also decrease the potential value of the electrode/solution interface. The BSA could avoid the passivation of the substrate by chelating effect according to Cheng and Roscoe results [15]. They found that the presence of BSA in PBS solution moved the E_{OCP} to negative values due to

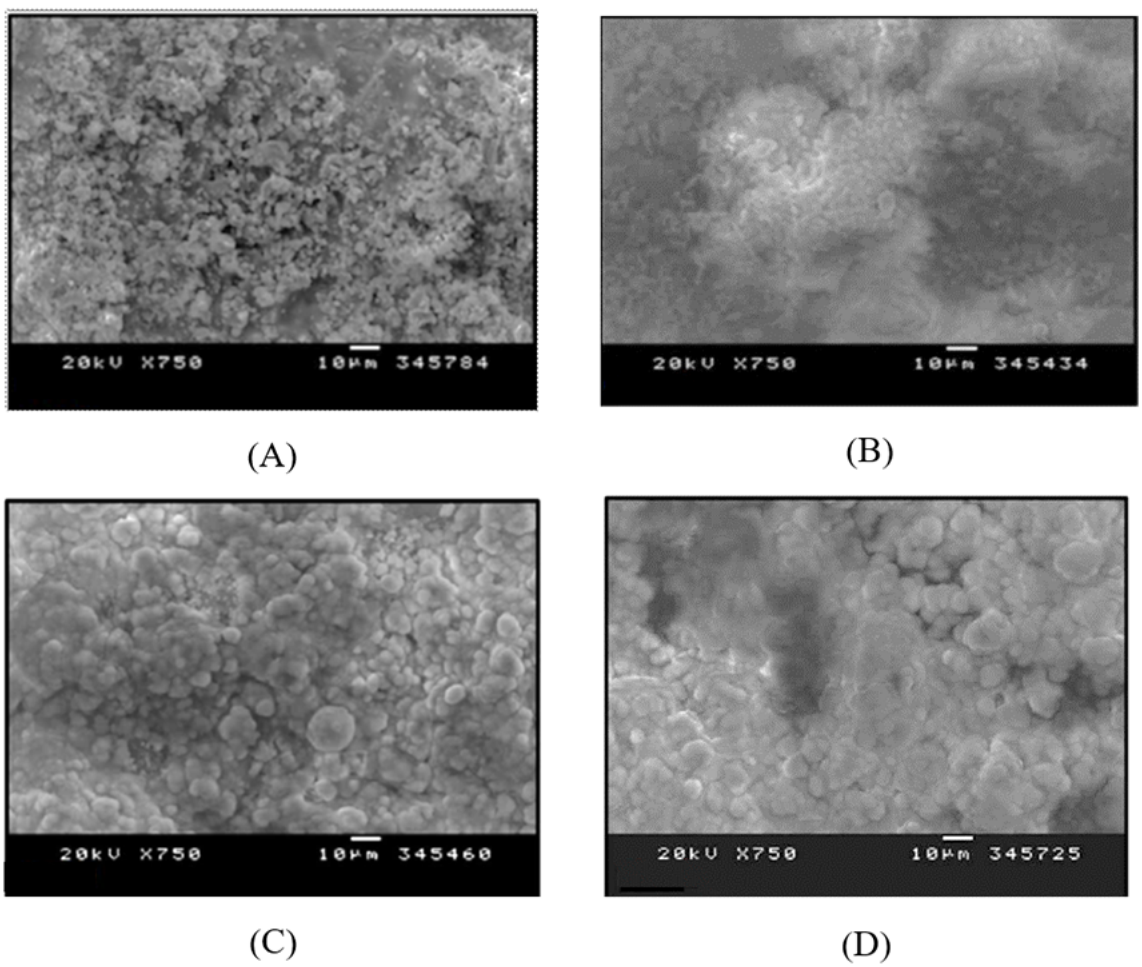

Figure 2. SEM images of 80-20 sample (A) as-sprayed and before immersion, and B, C and D, respectively, after 1, 7 and 28 days of immersion in non-aerated and unstirred Hanks' solution without BSA.

the chelating effect of the protein for calcium phosphate deposits prepared on Ti.

In order to know the electrochemical behavior of the uncoated and coated samples and the influence of BSA on the stability of the coatings, the E_{OCP} was measured each 24 h for 30 days (Fig. 1C). The sprayed coating layer of all samples was degraded after 30 days of immersion in Hanks' solution, remaining on the surface a thinner and porous layer, probably, containing natural apatite. The 80-20 sample was the lesser deteriorated during the test. It has been noticed that the starting E_{OCP} values were slightly different from the previous one. This difference was attributed to the fact that there was some time delayed carrying out the tests.

Figure 1C shows that all the samples have similar E_{OCP} values in the absence of BSA in solution, with small regular fluctuations of the E_{OCP} value for HA. These fluctuations are due to the dissolution-precipitation of the HA. During the dissolution of the HA, the local cells are actives and the alloy repassivation does not take place. Unlike, when apatite is depositing allows the system to repassivate.

According to our hypothesis, the E_{OCP} values of the 80-20 must evolve to the potential of the bare sample. This can clearly be seen for longer immersion times. At shorter times two opposite effects are taking place. One is the dissolution of the HA, being faster for the amorphous HA enhancing the local cells, and the other is the passivation of the substrate. Once the dissolution-precipitation of the HA reached equilibrium state the passivation of the substrate was measured, which gave the same E_{OCP} value as the bare sample. Also, small potential fluctuations were observed for 80-20, which were attributed to the dissolution-precipitation of HA, as in the case of HA sample.

The dissolution-precipitation of the HA can be followed in Figure 2. Figure 2A shows the free surface of the 80-20. The roughness of the surface corresponds to the deposition technology we used (around 4 µm). Figure 2B shows a less rough surface indicating that the dissolution and precipitation of freshly HA was taking place. The growing of this HA was clearly seen after 7 days of immersion (Fig. 2C). Several days later (28 days), a mixture between deposition and dissolution of HA was visible on the surface (Fig. 2D).

A continuous and slow decrease of the E_{OCP} values was observed for all samples when BSA was present. The chelating effect of the BSA plays now a key role in controlling the E_{OCP} values. Once the metallic oxide layer was dissolved, it could not be completely reconstructed because the metallic ions were captured by the chelating effect of BSA [15]. This chelating effect was much more pronounced for the bare metal than for the coated samples. On the other hand, we must still consider that the other effects explained before (dissolution-precipitation of HA) are still present and clearly seen in Fig. 1C.

R_p and E_{corr} values obtained from LP experiments after 24 h of immersion are in Table 2. The corrosion potential did not show many differences with E_{OCP} values, mainly due to the low scanning velocity employed. The polarization resistance is expected to be inversely proportional to the tendency to corrode, and gives an extra value that corroborates the results obtained by open circuit potential tests.

The presence of BSA in solution seemed that it did not have any effect on the corrosion resistance for TiAlV and 80-20 samples, but for HA sample, BSA increased R_p (at 24 h). The adhesion of the protein onto the surface of the coating might decrease the dissolution rate of the amorphous HA does decreasing the number of local cells, which slightly improved the R_p value. However, this value was still much lower than those for bare and 80-20 samples.

Cyclic polarization technique, after 24 h, enabled to overview the electrochemical behavior of bare and coated-Ti-based alloys in a large potential window (Fig. 3). The anodic current increased with increasing potential, but without a sharp and steady increase in the anodic current typical in pitting attack, and in the reverse scan the current density was always lower than in the direct one, which is characteristic of a more passivated system. Kwok et al. [12] found similar results by polarizing the HA-coated TiAlV electrodes fabricated by electrophoretic deposition up to 4 V/SCE and also Sousa

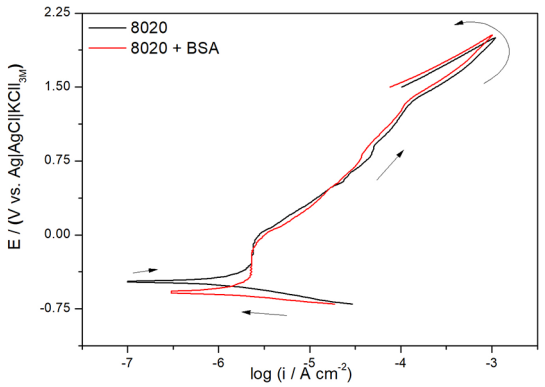

Figure 3. Cyclic polarization curves for the studied samples obtained in non-deaerated and unstirred Hanks' solution in the absence and presence of 4.2 g L^{-1} BSA, at 5 mV s^{-1} and 37 ºC.

Table 2. R_p, E_{corr} values for grit blasted TiAlV and as-sprayed HA-coated samples obtained after 24 h immersion in Hanks' solution without and with 4.2 g L^{-1} of BSA, at 37 °C.

	TiAlV		HA		80wt%HA-20wt%TiO_2	
	without BSA	with BSA	without BSA	with BSA	without BSA	with BSA
R_p/kΩ cm^2	721±58	673±75	107±25	224±46	335±37	328±16
E_{corr}/V	-0.156±0.024	-0.189±0.045	-0.351±0.006	-0.365±0.008	-0.235±0.005	-0.335±0.003

and Barbosa [25] who polarized the coating up to 3 V/SCE. The results shown in Fig. 3 agree with our hypothesis. The curve for the bare sample exhibited higher anodic current once the BSA was present in the solution, thus confirming the influence of the chelating effect. On the other hand, the current intensity of HA sample moved to lower values indicating that BSA was only blocking the surface of the HA and the chelating effect was negligible. However, Fig. 3C shows that there is no significant change in the current intensity for 80-20 sample. This behavior was attributed to the competition between the chelating and the adsorption effects. A small passivated zone was present, probably due to the presence of TiO_2 in the coating.

3.2 Electrochemical impedance studies

Figure 4A shows the experimental complex plane and Bode-phase angle diagrams for the 80-20 sample immersed in Hanks' solution as representative of the coatings studied. This sample was chosen because, as far as the authors know, studies with this composition were not found in literature. EIS diagrams of substrate were also performed for comparison and are shown in Figure 5.

The 80-20 sample did not present substantial changes in its capacitive loop (Fig. 4A). In phase angle diagram (Fig. 4B) two time constants were observed at the region from the medium to low frequencies (MF/LF): one time constant related to the dielectric proprieties of the coating at the MF domain and another at the LF region related to the interfacial processes. The phase angle at MF is around -60º and decreased mainly up to 6 days. As mentioned above

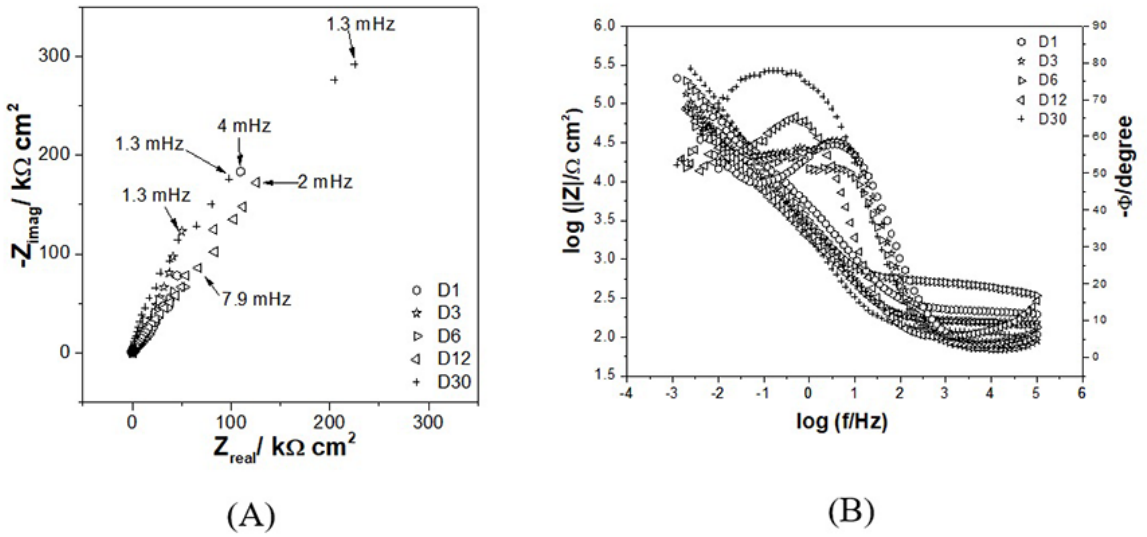

Figure 4. Experimental complex plane and Bode plots for 80-20 sample in non-aerated and unstirred Hanks' solution without BSA for 30 days of immersion at 37 ºC: (A) complex plane plots; (B) Bode - phase angle *vs*. log *f* and impedance modulus *vs*. log *f* plots.

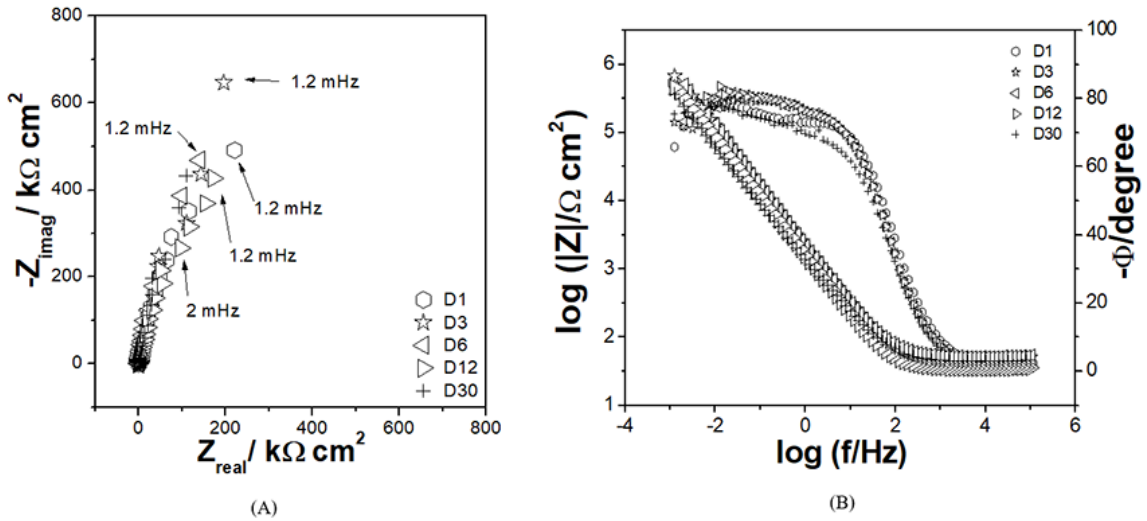

Figure 5. Experimental complex plane and Bode plots for bare substrate in non-aerated and unstirred Hanks' solution without BSA for 30 days of immersion at 37 ºC: (A) complex plane plots; (B) Bode - phase angle *vs*. log *f* and impedance modulus *vs*. log *f* plots.

the phenomenon occurring is the dissolution-precipitation of hydroxyapatite to reach equilibrium, but as it will be seen coating was strongly damaged at the end of experiments due to the dissolution process, which made the influence of the coating to decrease as the immersion time increased. The time constant at low frequency (around 5 mHz) moved to higher frequency for long immersion times, indicating that the charge transfer process was facilitated probably due to the dissolution of the hydroxyapatite.

The bare substrate (Fig. 5) did not display significant changes on its capacitive loop (Fig. 5A) and its impedance modulus as well (Fig. 5B). The evolution of that system with time is demonstrated, for instance, by the changes in the Bode diagrams phase angle (Fig. 5B). It was observed a small decrease in the phase angle value at around 1 Hz while a slightly increase was seen at around 1 mHz. The frequency range with a high capacitive feature was lower than that for titanium (material to be passivated easily), probably due to the dissolution of Al and V alloying elements, which was indicated by a decrease of the phase angle value at very low frequency.

The complex plane plots of the HA sample (Fig. 6A) showed a gradual grow of the capacitive loop which could be related to development of oxide at the bottom of the coating pores, already discussed above. This was also indicated in the Bode plots (Fig. 6B), in which two distinct time constants were displayed and were attributed to the same phenomena as in the case of 80-20 sample. As time elapse, the phase angle of the LF time constant increased till it reached values similar to the bare substrate response at long immersion times.

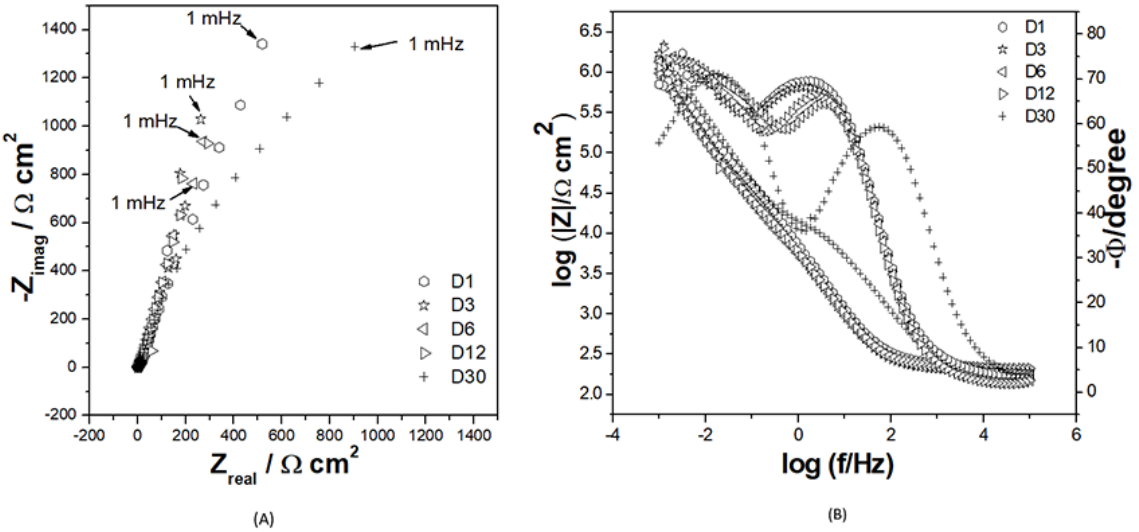

Figure 6. Experimental complex plane and Bode plots for HA sample in non-aerated and unstirred Hanks' solution without BSA for 30 days of immersion at 37 ºC: (A) complex plane plots; (B) Bode - phase angle *vs*. log *f* and impedance modulus *vs*. log *f* plots.

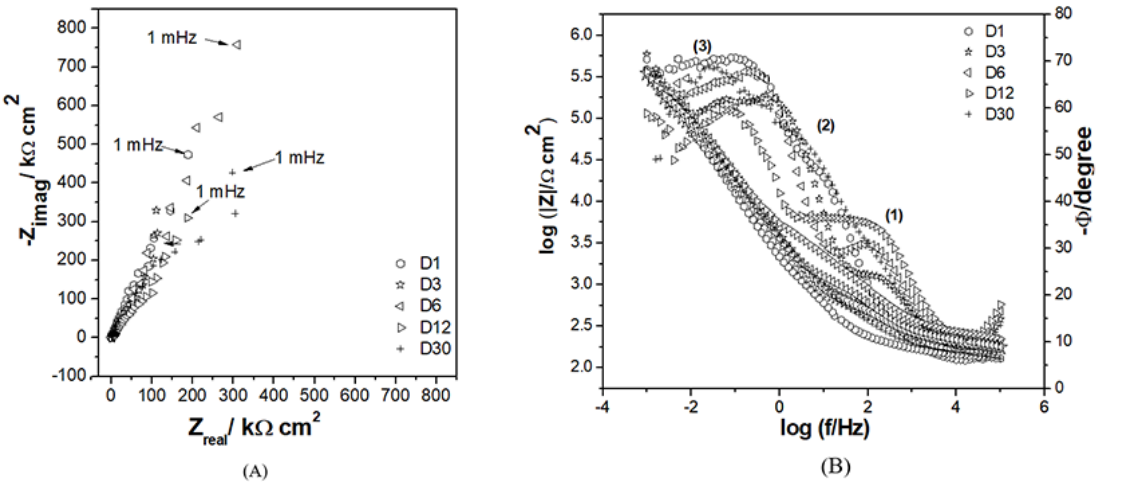

Figure 7. Impedance diagrams for 80-20 sample in non-aerated and unstirred Hanks' solution with 4.2 g L^{-1} BSA for 30 days of immersion at 37 ºC: (A) complex plane plots; (B) Bode - phase angle *vs*. log *f* and impedance modulus *vs*. log *f* plots.

Figure 7 shows the experimental EIS diagrams for 80-20 sample immersed in Hanks' solution with 4.2 g L^{-1} BSA. For 80-20 sample, the complex plane plots showed higher capacitive loop in the presence of BSA (Fig. 7A) than in its absence (Fig. 4A), indicating an increase in the impedance of the system. Previous work [18] have considered that the presence of BSA could increase the corrosion resistance of the system due to its adsorption on the coating and metal surface [35], at least at short times, where the hydroxyapatite layer was not dissolved yet. When the system was polarized during the cyclic polarization experiments after 24 h of immersion, it was observed lower current density for a large potential interval in the presence of BSA for both 80-20 and HA samples (Fig. 3), but a decrease of resistance at around the open circuit potential for freshly prepared samples (Table 2). The samples used for impedance studies were stored at room conditions before tests which might developed more resistant oxide film at the bottom of the pores compared to the freshly prepared samples. Therefore, it is possible that the expected chelating effect around the open circuit potential is less important than the effect of BSA adsorption on the coating, which may lead to an increase of both the impedance and, consequently, a decrease of the current or corrosion. In phase angle diagrams (Fig. 7B) three frequency regions could be identified. At high frequency (region 1) a time constant appeared after 3 days of immersion and increased its influence with time up

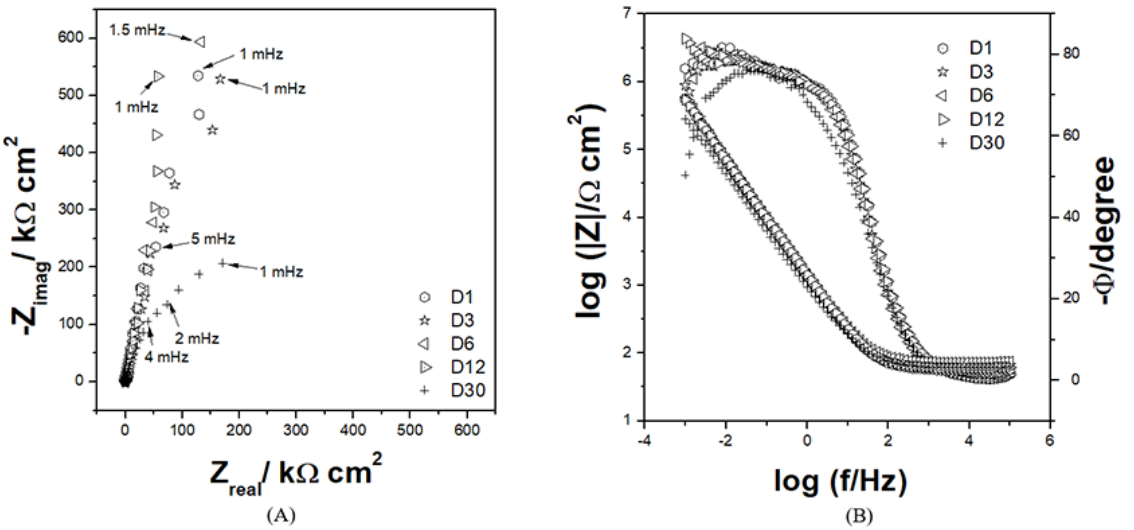

Figure 8. Impedance diagrams for bare electrode in non-aerated and unstirred Hanks' solution with 4.2 g L^{-1} BSA for 30 days of immersion at 37 ºC: (A) complex plane plots; (B) Bode - phase angle *vs*. log *f* and impedance modulus *vs*. log *f* plots.

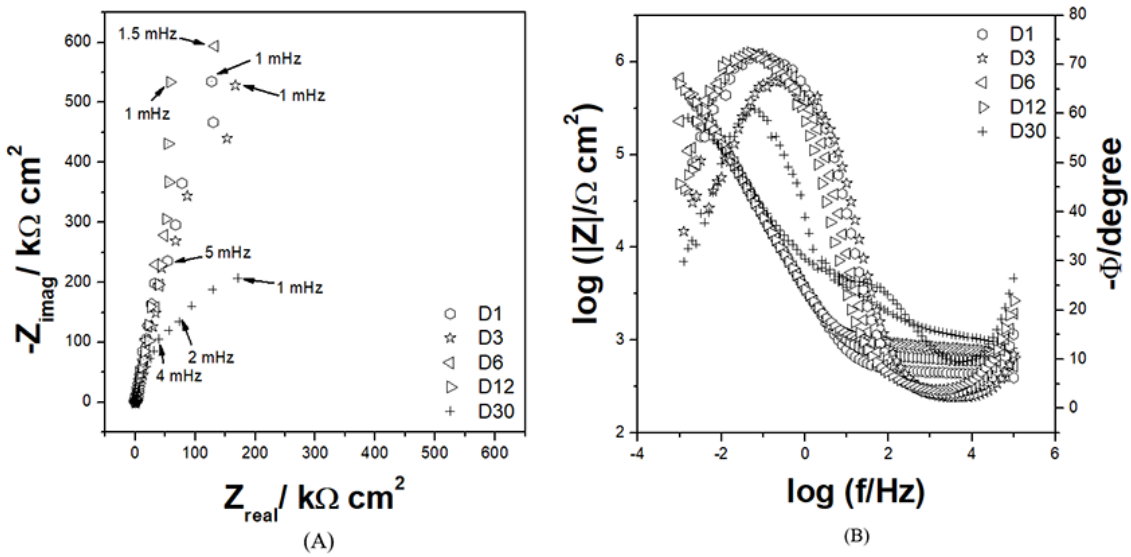

Figure 9. Impedance diagrams for HA sample in non-aerated and unstirred Hanks' solution with 4.2 g L^{-1} BSA for 30 days of immersion at 37 ºC: (A) complex plane plots; (B) Bode - phase angle *vs*. log *f* and impedance modulus *vs*. log *f* plots.

to 12 days and shifted to lower frequency for t > 18 days, suggesting that the adsorption of BSA is time-dependent. The other phenomenon is the dissolution-precipitation mainly of amorphous hydroxyapatite during the first hours of immersion. Region 2 was attributed to hydroxyapatite layer and for t > 18 days both 1 and 2 regions merger each other. In region 3, the interfacial processes emerged and was more evident for longer times as a consequence of the damaging of hydroxyapatite layer. The comparison of Figs. 4E and 7E indicated that the interfacial processes were anticipated by the presence of BSA mainly for longer times, which could be related to the increase of the chelating effect. The last one is known to accelerate the hydroxyapatite dissolution [15]. The modulus of impedance *versus* frequency (Fig. 7B) shows the same tendency observed for phase angle plots.

EIS diagrams for the titanium alloy immersed in Hanks' solution with 4.2 g L^{-1} BSA are shown in Fig. 8. Complex plane diagrams (Fig. 8A) show very high impedance which decreases with immersion time and suggest the presence of one time constant. The phase angle plot for the bare substrate (Fig. 8B), in the presence of BSA, displayed overlapped time constants pointing to a competition between adsorption / chelating effects of BSA, which may accelerated interfacial process for longer times due to the increase of the chelating effect mainly relating with trapping of vanadium ions [43]. However, it presented a decrease of the capacitive loop (Fig. 8A) after 12 days of immersion characteristic of an activation of the surface by the enlargement of the pores due to chelating effect removing the alloying elements and avoiding thickening of the titanium oxide layer. In the same direction, the modulus of impedance *versus* frequency (Fig. 8C and 8F) shows a slightly decrease of impedance at low frequencies mainly for immersion times > 12 days.

EIS diagrams for the hydroxyapatite coating immersed in Hanks' solution with 4.2 g L^{-1} BSA are shown in Fig. 9). Complex plane diagrams (Fig. 9A) show impedance values lower than the substrate and the 80-20 samples probably due to the high chelating effect of BSA. For the same reason the modulus of impedance versus frequency (Fig. 9B) show a more pronounced decrease of impedance than the others at low frequencies. Hydroxyapatite coating displayed at least 2 time constants, one related to coating response (MF) and the other to the interfacial process at metal surface (LF) (Fig. 9B). After 3 days of immersion, they evolved to overlapped time constants resembling the substrate response. Then, after 14 days the HF phase angle decreased and another time constant appeared at MF pointing that something might be covering the exposed area. The gradual increase of the solution resistance could be related to the change in the ionic strength [18] with the high dissolution of hydroxyapatite.

The observation of the samples surface after 30 days of immersion showed that HA coating in the presence and absence of BSA and HA-TiO_2 coating in the presence of BSA were strongly damaged mainly at the top and at the coating/substrate interface. The HA-TiO_2 coating in the absence of BSA in solution became highly porous with the coating/substrate interface corroded as shown in Fig. 6. In that image is possible to see the depth difference between different regions of the sample, pointing to higher dissolution of the coating in some areas. These miscarried areas in addition of the cracks into the coatings corroborate the EIS experimental data, since the coating response did not appear for long immersion times, and typically lost influence with time.

Two main processes are mainly present in these coatings, but with different intensity depending on the coating and/ or the presence of BSA: the dissolution-precipitation of amorphous HA phase is more significant at the short immersion period and an equilibrium seems to be reached after some time, but with some damage of the coating, indicating that the addition of TiO_2 increases the stability of HA; the presence of BSA in solution put in evidence the chelating effect which increases the HA dissolution and accelerates the damage to the coating. As consequence of this dissolution, at the end of the test (around 30 days) the bare electrode features domain the electrochemical response mainly for HA sample, and the solution becomes cloudy due to the presence of hydroxyapatite into the solution. For the HA sample, after 28 days of immersion precipitates are visible at the bottom of the cell. As the working electrode is horizontally placed at the bottom of the electrochemical cell, it is possible that some deposit is formed at the surface increasing the impedance of the system. By obvious reason the coatings thickness were not measured after 30 days of test in Hanks´solution.

4. Conclusions

The results obtained for HVOF produced hydroxyapatite coatings in Hanks' solution for 30 days of immersion allow drawing the following conclusions:

- The HA-TiO_2 coating (80-20 sample) was the only one that showed a clear passive region from around -0.4 V to 0 V *vs.* Ag/AgCl/KCl_{3M} in the presence and absence of BSA, indicating the beneficial influence of the addition of TiO_2 to the HA coating stability.
- The HA coating is strongly damaged due to dissolution-precipitation process with immersion time and after 18 days in the absence and 6 days in the presence of bovine serum albumin (BSA) in Hanks' solution, it lost influence on the impedance response, resemble the bare substrate behavior.
- The addition of TiO_2 to the HA coating delayed the HA dissolution, increasing the coating stability. The influence of the coating on the EIS diagrams disappeared after 18 days for HA and after 24 days of immersion for 80-20 sample.

- In the presence of BSA in Hanks' solution the addition of TiO_2 to the HA coating delayed the influence of the coating in EIS diagrams from 6 days for HA to 24 days for HA-TiO_2 coatings.
- Our results also indicated that BSA in Hanks' solution diminishes the stability of the metallic oxide layer present on the Ti-based alloy and accelerates the hydroxyapatites coatings dissolution mainly for longer immersion times.

5. Acknowledgements

The authors thank the CNPq (Conselho Nacional de Pesquisa, Brazil) for the researcher scholarship (Proc. 305890/2010-7) and FUNDECT (Proc. 23/200.693/2012).

6. References

1. Tomashov ND, Chernova GP, Ruscol YS, Ayuyan GA. The passivation of alloys on titanium bases. *Electrochimica Acta.* 1974;19(4):159-172.

2. Charrière E, Terrazzoni S, Pittet C, Mordasini P, Dutoit M, J. Lemaître J, et al. Mechanical characterization of brushite and hydroxyapatite cements. *Biomaterials*. 2001;22(21):2937-2945.

3. Goyenvalle E, Aguado E, Nguyen JM, Passuti N, Le Guehennec L, Layrolle P, et al. Osteointegration of femoral stem prostheses with a bilayered calcium phosphate coating. *Biomaterials.* 2006;27(7):1119-1128.

4. Melero H, Torrell M, Fernández J, Gomes JR, Guilemany JM. Tribological characterization of biocompatible HAp-TiO_2 coatings obtained by high velocity oxy-fuel spray. *Wear.* 2013;305(1-2):8-13.

5. Kumar A, Biswas K, Basu B. On the toughness enhancement in hydroxyapatite-based composites. *Acta Materialia.* 2013;61(14):5198-5215.

6. Chien CY, Liu TY, Kuo WH, Wang MJ, Tsai WB. Dopamine-assisted immobilization of hydroxyapatite nanoparticles and RGD peptides to improve the osteoconductivity of titanium. *Journal of Biomedical Materials Research. Part A.* 2013;101(3):740-747.

7. Kwok CT, Wong PK, Cheng FT, Man HC. Characterization and corrosion behavior of hydroxyapatite coatings on Ti6Al4V fabricated by electrophoretic deposition. *Applied Surface Science.* 2009;255(13-14):6736-6744.

8. Guilemany JM, Fernández J, Espallargas N, Suegama PH, Benedetti AV. Influence of spraying parameters on the electrochemical behaviour of HVOF thermally sprayed stainless steel coatings in 3.4% NaCl. *Surface and Coatings Technology.* 2006;200(9):3064-3072.

9. Silva PL, Santos JD, Monteiro FJ, Knowles JC. Adhesion and microstructural characterization of plasma-sprayed hydroxyapatite/glass ceramic coatings onto Ti-6A1-4V substrates. *Surface and Coatings Technology.* 1998;102(3):191-196.

10. Lima RS, Khor KA, Li H, Cheang P, Marple BR. HVOF spraying of nanostructured hydroxyapatite for biomedical applications. *Materials Science and Engineering: A.* 2005;396(1-2):181-187.

11. Zyman Z, Cao Y, Zhang X. Periodic crystallization effect in the surface layers of coatings during plasma spraying of hydroxyapatite. *Biomaterials.* 1993;14(15):1140-1144.

12. Ji H, Ponton CB, Marquis PM. Microstructural characterization of hydroxyapatite coating on titanium. *Journal of Materials Science: Materials in Medicine.* 1992;3(4):283-287.

13. Cabrini M, Cigada A, Rondelli G, Vicentini B. Effect of different surface finishing and of hydroxyapatite coatings on passive and corrosion current of Ti6Al4V alloy in simulated physiological solution. *Biomaterials.* 1997;18(11):783-787.

14. Nie X, Leyland A, Matthews A. Deposition of layered bioceramic hydroxyapatite/TiO_2 coatings on titanium alloys using a hybrid technique of micro-arc oxidation and electrophoresis. *Surface and Coatings Technology.* 2000;125(1-3):407-414.

15. Cheng X, Roscoe SG. Corrosion behavior of titanium in the presence of calcium phosphate and serum proteins. *Biomaterials.* 2005;26(35):7350-7356.

16. Drevet R, Aaboubi O, Benhayoune H. In vitro corrosion behavior of electrodeposited calcium phosphate coatings on Ti6Al4V substrates. *Journal of Solid State Electrochemistry.* 2012;16(9):3069-3077.

17. Zhang B, Kwok CT. Hydroxyapatite-anatase-carbon nanotube nanocomposite coatings fabricated by electrophoretic codeposition for biomedical applications. *Journal of Materials Science: Materials in Medicine.* 2011;22(10):2249-2259.

18. Vasilescu C, Drob P, Vasilescu E, Demetrescu I, Ionita D, Prodana M, et al. Characterisation and corrosion resistance of the electrodeposited hydroxyapatite and bovine serum albumin/hydroxyapatite films on Ti-6Al-4V-1Zr alloy surface. *Corrosion Science.* 2011;53(3):992-999.

19. Zhou X, Mohanty P. Electrochemical behavior of cold sprayed hydroxyapatite/titanium composite in Hanks' solution. *Electrochimica Acta.* 2012;65:134-140.

20. Lee CK. Fabrication, characterization and wear corrosion testing of bioactive hydroxyapatite/nano-TiO_2 composite coatings on anodic Ti-6Al-4V substrate for biomedical applications. *Materials Science and Engineering: B.* 2012;177(11):810-818.

21. Zhou X, Siman R, Lu L, Mohanty P. Argon atmospheric plasma sprayed hydroxyapatite/Ti composite coating for biomedical applications. *Surface and Coatings Technology.* 2012;207:343-349.

22. Singh G, Singh H, Sidhu BS. Characterization and corrosion resistance of plasma sprayed HA and HA-SiO_2 coatings on Ti-6Al-4V. *Surface and Coatings Technology.* 2013;228:242-247.

23. Hiromoto S, Mischler S. The influence of proteins on the fretting-corrosion behaviour of a Ti6Al4V alloy. *Wear.* 2006;261(9):1002-1011.

24. Feliu V, González JA, Adrade C, Feliu S. Equivalent circuit for modelling the steel-concrete interface. II. Complications in applying the stern-geary equation to corrosion rate determinations. *Corrosion Science.* 1999;40(6):995-1006.

25. Sousa SR, Barbosa MA. Effect of hydroxyapatite thickness on metal ion release from Ti6Al4V substrates. *Biomaterials.* 1996;17(4):397-404.

26. Souto RM, Laz MM, Reis RL. Degradation characteristics of hydroxyapatite coatings on orthopaedic TiAlV in simulated physiological media investigated by electrochemical impedance spectroscopy. *Biomaterials.* 2003;24(23):4213-4221.

27. Barsoukov E, Macdonald RJ, eds. *Impedance Spectroscopy Theory, Experiment, and Applications.* 2nd ed. Hoboken: John Wiley & Sons; 2005.

28. Orazem ME, Tribollet B. *Electrochemical Impedance Spectroscopy.* Hoboken: John Wiley & Sons; 2012.

29. Lvovich VF. *Impedance-Spectroscopy: Applications to Electrochemical and Dielectric Phenomena.* Hoboken: John Wiley & Sons; 2012.

30. Liu Y, Huang J, Li H. Nanostructural Characteristics of Vacuum Cold-Sprayed Hydroxyapatite/Graphene-Nanosheet Coatings for Biomedical Applications. *Journal of Thermal Spray Technology.* 2014;23(7):1149-1156.

31. Liu Y, Dang Z, Wang Y, Huang J, Li H. Hydroxyapatite/graphene-nanosheet composite coatings deposited by vacuum cold spraying for biomedical applications: Inherited nanostructures and enhanced properties. *Carbon.* 2014;67:250-259.

32. Metoki N, Leifenberg-Kuznits L, Kopelovich W, Burstein L, Gozin M, Eliaz N. Hydroxyapatite coatings electrodeposited at near-physiological conditions. *Material Letters.* 2014;119:24-27.

33. Levingstone TJ, Ardhaoui M, Benyounis K, Looney L, Stokes JT. Plasma sprayed hydroxyapatite coatings: Understanding process relationships using design of experiment analysis. *Surface and Coatings Technology.* 2015;283:29-36.

34. Pouilleau J, Devilliers D, Garrido F, Durand-Vidal S, Mahé E. Structure and composition of passive titanium oxide films. *Materials Science and Engineering: B.* 1997;47(3):235-243.

35. Sousa SR, Moradas-Ferreira P, Saramago B, Melo LV, Barbosa MA. Human Serum Albumin Adsorption on TiO2 from Single Protein Solutions and from Plasma. *Langmuir.* 2004;20(22):9745-9754.

36. Lavos-Valereto IC, Costa I, Wolynec S. The electrochemical behavior of Ti-6Al-7Nb alloy with and without plasma-sprayed hydroxyapatite coating in Hank's solution. *Journal of Biomedical Materials Research.* 2002;63(5):664-670.

37. Contu F, Elsener B, Böhni H. A study of the potentials achieved during mechanical abrasion and the repassivation rate of titanium and Ti6Al4V in inorganic buffer solutions and bovine serum. *Electrochimica Acta.* 2004;50(1):33-41.

38. Milošev I, Metikoš-Huković M, Strehblow HH. Passive film on orthopaedic TiAlV alloy formed in physiological solution investigated by X-ray photoelectron spectroscopy. *Biomaterials*. 2000;21(20):2103-2113.

39. Roland T, Pelletier H, Krier J. Scratch resistance and electrochemical corrosion behavior of hydroxyapatite coatings on Ti6Al4V in simulated physiological media. *Journal of Applied Electrochemistry.* 2013;43(1):53-63.

40. Mohamed SG, Abdeltawab AA, Shoeib MA. Corrosion behaviour and bioactivity of electrophoretically deposited hydroxyapatite on titanium in physiological media (Hanks' solution). *Materials Science-Poland.* 2012;30(3):231-239.

41. Melero H, Fernández J, Dosta S, Guilemany JM. Caracterización de nuevos recubrimientos biocompatibles de hidroxiapatita-TiO_2 obtenidos mediante Proyección Térmica de Alta Velocidad. *Boletín de la Sociedad Española de Cerámica y Vidrio.* 2011;50(2):59-64.

42. Zhang Z, Dunn MF, Xiao TD, Tomsia AP, Saiz E. Nanostructured Hydroxyapatite Coatings for Improved Adhesion and Corrosion Resistance for Medical Implants. *MRS Proceedings*. 2001;703.

43. MacDonald DE, Rapuano BE, Deo N, Stranick M, Somasundaran P, Boskey AL. Thermal and chemical modification of titanium-aluminum-vanadium implant materials: effects on surface properties, glycoprotein adsorption, and MG63 cell attachment. *Biomaterials.* 2004;25(16):3135-3146.